

Multistage reaction pathways in detonating high explosives

Ying Li, Rajiv K. Kalia, Aiichiro Nakano, Ken-ichi Nomura, and Priya Vashishta

Citation: *Applied Physics Letters* **105**, 204103 (2014); doi: 10.1063/1.4902128

View online: <http://dx.doi.org/10.1063/1.4902128>

View Table of Contents: <http://scitation.aip.org/content/aip/journal/apl/105/20?ver=pdfcov>

Published by the [AIP Publishing](#)

Articles you may be interested in

[Initial chemical events in shocked octahydro-1,3,5,7-tetranitro-1,3,5,7-tetrazocine: A new initiation decomposition mechanism](#)

J. Chem. Phys. **136**, 044516 (2012); 10.1063/1.3679384

[Combining ab initio quantum mechanics with a dipole-field model to describe acid dissociation reactions in water: First-principles free energy and entropy calculations](#)

J. Chem. Phys. **132**, 074112 (2010); 10.1063/1.3317398

[Modeling deflagration-to-detonation transition in granular explosive pentaerythritol tetranitrate](#)

J. Appl. Phys. **104**, 043519 (2008); 10.1063/1.2970168

[Simulated thermal decomposition and detonation of nitrogen cubane by molecular dynamics](#)

J. Chem. Phys. **127**, 134503 (2007); 10.1063/1.2779877

[Interplay of explosive thermal reaction dynamics and structural confinement](#)

J. Appl. Phys. **101**, 074901 (2007); 10.1063/1.2713090



Multistage reaction pathways in detonating high explosives

Ying Li,^{1,2} Rajiv K. Kalia,¹ Aiichiro Nakano,¹ Ken-ichi Nomura,¹ and Priya Vashishta¹

¹*Collaboratory for Advanced Computing and Simulations, Department of Physics and Astronomy, Department of Computer Science, and Department of Chemical Engineering and Materials Science, University of Southern California, Los Angeles, California 90089-0242, USA*

²*Argonne Leadership Computing Facility, Argonne National Laboratory, Argonne, Illinois 60439, USA*

(Received 6 October 2014; accepted 3 November 2014; published online 19 November 2014)

Atomistic mechanisms underlying the reaction time and intermediate reaction products of detonating high explosives far from equilibrium have been elusive. This is because detonation is one of the hardest multiscale physics problems, in which diverse length and time scales play important roles. Here, large spatiotemporal-scale reactive molecular dynamics simulations validated by quantum molecular dynamics simulations reveal a two-stage reaction mechanism during the detonation of cyclotrimethylenetrinitramine crystal. Rapid production of N₂ and H₂O within ~10 ps is followed by delayed production of CO molecules beyond ns. We found that further decomposition towards the final products is inhibited by the formation of large metastable carbon- and oxygen-rich clusters with fractal geometry. In addition, we found distinct unimolecular and intermolecular reaction pathways, respectively, for the rapid N₂ and H₂O productions. © 2014 AIP Publishing LLC. [<http://dx.doi.org/10.1063/1.4902128>]

Many high-explosive (HE) materials are organic molecular solids that contain C, H, O, and N atoms.^{1–3} Detonation of these HEs involves complex interplay between mechanical shock loading, thermo-mechanical response, and induced chemistry.^{4,5} The process starts when the leading shock front compresses and heats up the unreacted material. For sufficiently strong shock, the high temperature and pressure trigger the chemical decomposition of the HE. Once initiated, the HE spontaneously reacts to release energy in supersonic detonation waves. Immediately behind the detonation wave front, the density and pressure increase, in the form of von Neumann spike, then decrease as the chemical reactions progress and the material expands into the reaction zone. The length of this reaction zone, as well the associated reaction time, is a fundamental quantity that dictates various important properties of HEs such as sensitivity.⁶ The reaction time in turn is essentially determined by what intermediated reaction products are produced, i.e., the reaction pathways.^{6–8} It has been suggested that the slow formation time of certain products play an essential role in determining the reaction time of some HEs.^{6,9,10} However, the molecular processes that determine the reaction time are largely unknown.⁶

Cyclotrimethylenetrinitramine (C₃H₆N₆O₆ or RDX) is one of the most powerful HEs, yet with good stability under ambient conditions. Consequently, this archetypal HE has been studied extensively both experimentally^{11–14} and theoretically.^{15–18} In particular, the reaction pathways of a single RDX molecule have been mapped out in detail.¹⁹ The final products of RDX detonation include carbon monoxide (CO), nitrogen (N₂), and steam (H₂O).^{20,21} The reaction time for RDX detonation has been inferred from electrical conductivity measurements to be over ns with the corresponding reaction zone width exceeding μm.^{22–24} Apart from the overall reaction time, however, little is known about the reaction pathways within ns. Thus, a serious knowledge gap exists on sub-ns reaction dynamics of RDX under high-pressure, high-temperature conditions.^{11,25,26}

Experimental research on explosion (e.g., shock-induced phase transition and shock-induced chemistry) has been a challenge.^{27,28} Due to the advancement of experiments, reactions under shock can now be observed with extremely fine spatial and temporal resolutions.^{29–31} The key scientific questions are: What is the reaction time for the detonation of RDX solid, and what are the intermediate reaction products that determine it? It has been realized that the chemical dynamics behind the shock front in energetic materials located in a ~100 nm thin layer and on the ~100 ps time scale is critical to understand microscopic details of detonation.^{31,32} Unfortunately, no MD simulation capable of describing chemical reactions has been performed to encompass the large length (~100 nm) and time (~100 ps) scales.³³ In order to overcome this computational challenge, we have developed a scalable parallel implementation of reactive force-field (ReaxFF) MD simulation based on spatial decomposition and message passing.³⁴ To describe chemical reactions with moderate computational costs, the first principles-based ReaxFF allows bond breaking and bond formation through reactive bond orders and dynamical charges by employing an electronegativity-equalization scheme.^{35,36}

In this paper, we present ReaxFF MD simulations validated by quantum molecular dynamics (QMD) simulations to study shock-induced detonation of RDX. Simulation results provide the first evidence of the formation of large carbon- and oxygen-rich clusters as intermediate products. This inhibits the production of one of the final products, CO. As a result, the detonation of RDX proceeds in two stages: Rapid production of N₂ and H₂O within tens of ps, followed by delayed CO production in ns. Furthermore, distinct unimolecular and intermolecular reaction pathways are found, respectively, for the rapid N₂ and H₂O productions.

The initial system setup is composed of 168 × 5 × 5 unit cells of RDX crystal in an MD simulation box of dimensions 222.8 × 5.787 × 5.354 nm³ at room temperature. Real HEs are defective (e.g., plasticizer bonded, wax added, and

porous),¹⁴ and these heterogeneities lead to complex multidimensional flows even in macroscopically unidirectional detonation.³⁷ In particular, voids cause localized hot spots, which essentially drive the decomposition reaction.³⁸ To mimic this effect, a void of size $3 \times 3 \times 3$ unit cells is randomly inserted in every $5 \times 5 \times 6$ unit cells of the RDX crystal. Figures 1(a) and 1(b) show the atomic structure of an RDX molecule and the configuration of the RDX crystalline unit cell, respectively. The number of RDX molecules inside the system is 27 552, amounting to the total number of atoms to be 578 592.

Starting from this initial configuration, we perform MD simulations with a time step of 0.1 fs up to 70 ps. Figure 1(c) shows a schematic diagram of shock loading. To model the shock wave and subsequent detonation and expansion, we employ a planar impact loading by a rigid-wall piston with the speed of $v_p = 6$ km/s from the right end onto the system. When the shock front hits the rigid wall at the left end of the simulation box, it is reflected back to the right. It takes about 11 ps for the shock wave to travel for a distance of 110 nm, indicating the shock speed of ~ 10 km/s. This is above the RDX detonation speed of 8.75 km/s, suggesting an overdriven detonation.³⁹ After the shock front bounces back towards right, the piston is removed to allow the detonated RDX to expand freely. The expansion continues until the volume of the system becomes three times the original value. Figure 1(d) shows a colored map of the temperature as a function of the x position and time. The initial length of RDX is $X_0 = 222.8$ nm. The highest temperature of the system reaches 3000 K near the shock front (shown as diamond-shaped red spots in Fig. 1(d)) before 20 ps, and during compression at 20–30 ps. A similar

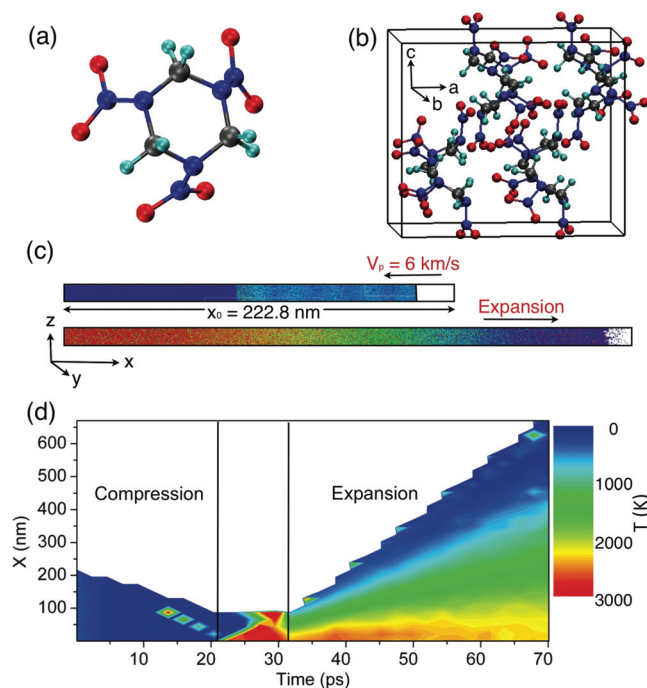
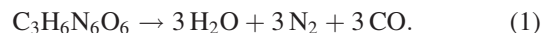


FIG. 1. (a) RDX molecule, where gray, cyan, blue, and red spheres represent C, H, N and O atoms, respectively. (b) RDX unit cell. The 8-molecule (or 168-atom) unit cell has the lattice parameters of $a = 13.182$ Å, $b = 11.574$ Å, $c = 10.709$ Å, and $\alpha = \beta = \gamma = 90^\circ$. (c) Schematic diagram of shock-induced detonation and propagation in the [100] crystallographic direction. (d) Colored map of temperature as a function of the x position and time.

colored map for pressure distribution is shown in Fig. S1 in the supplementary material.⁴⁰

To study the chemical reaction pathways, we have performed fragment analysis, where a cluster of covalently bonded atoms is counted as a molecule. Here, a pair of atoms are considered connected if the bond order of the pair is greater than 0.3 (Ref. 41) and their distance is less than a critical value slightly larger than the corresponding covalent bond length. Figure 2 shows the number of molecular products as a function of time. These include the final products (H_2O , N_2 , and CO) of the overall reaction of RDX decomposition



Among the final products, we observe rapid production of N_2 and H_2O during the initial expansion phase followed by plateaus in the later stage. We also observe a very slow production of CO . To estimate the time constant τ_α for the production of the α -th final product ($\alpha = \text{H}_2\text{O}$, N_2 , CO), we fit the yield of the corresponding molecular fragments as a function of time as

$$\eta_\alpha(t) = 1 - \exp(-t/\tau_\alpha). \quad (2)$$

Here, $\eta_\alpha(t)$ is defined as the ratio of the observed number of the α -th fragments at time t to the asymptotic number for $t \rightarrow \infty$ expected from Eq. (1) (The detailed procedures for estimating the time constants and associated error bars are described in the supplemental material.⁴⁰). The fitting produces $\tau_{\text{N}_2} = 10 \pm 2$ ps, $\tau_{\text{H}_2\text{O}} = 30 \pm 4$ ps, and $\tau_{\text{CO}} = 900 \pm 400$ ps. Namely, the detonation reaction proceeds in two stages: Rapid production of N_2 and H_2O , followed by much slower production of CO . The rapid production of N_2 and H_2O at an early stage of detonation is consistent with earlier simulation by Strachan *et al.*⁴² In their simulation for 5 ps, the dominant products were N_2 and H_2O . Also, slightly different multistage reactions were observed experimentally by Anisichkin⁴³ for a related HE, RDX/TNT mixture, using an isotope tracer method. In order to verify that the two-stage reaction is not an artifact of the simulation schedule, we have performed another simulation using a different schedule. Figure S2 shows the number of molecular fragments as a function of time for the

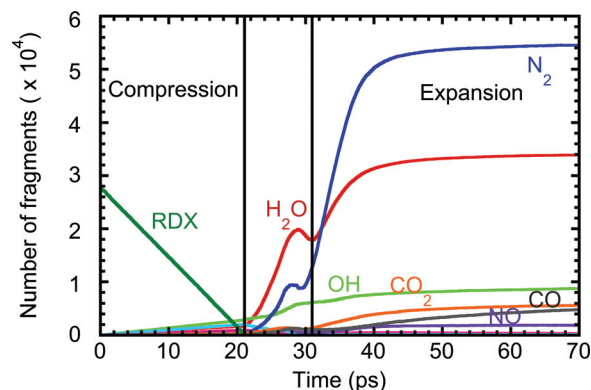


FIG. 2. Number of molecular fragments as a function of time. As the shock front begins to reflect, a rapid production of H_2O , OH , and N_2 is observed. Shortly after the expansion phase begins, various chemical products such as CO , CO_2 , and NO are produced.

alternative simulation, which also exhibits two distinct reaction rates.⁴⁰ In addition, we have performed another simulation, in which the original schedule was applied to another HE, triaminotrinitrobenzene ($C_6H_6O_6N_6$ or TATB). For TATB, we have not observed a separation of time scales. These results indicate that the two-stage reaction is an intrinsic property of RDX.

In order to identify the reaction pathways for the rapid production of N_2 and H_2O , we backtrack where the atoms composing individual N_2 and H_2O molecules originate in the initial configuration of the simulation. For some of the N_2 and H_2O products, all the atoms that constitute a molecule originate from a single RDX molecule, i.e., unimolecular pathways. For others, atoms from different RDX molecules form N_2 and H_2O molecules, i.e., intermolecular pathways. Examples are shown in Fig. 3, where the H, O, and N atoms that constitute the circled N_2 and H_2O products in Fig. 3(b) are highlighted, respectively, with green, yellow, and magenta colors in the initial configuration in Fig. 3(a). In Fig. 3(a), one green H atom belongs to a $-CH_2$ group of one RDX molecule, while another green H atom belongs to a $-CH_2$ group of another RDX molecule and one yellow O atom belongs to an $-NO_2$ group of the latter RDX molecule. Immediately after the reversed shock front traveling rightward passes, cleavages of C and H atoms from $-CH_2$ groups and N and O atoms from $-NO_2$ group release the highlighted H and O atoms, which together form the H_2O molecule circled in Fig. 3(b), signifying an intermolecular pathway. In contrast, for the N_2 molecule circled in Fig. 3(b), both magenta N atoms composing the N-N bond originate from one

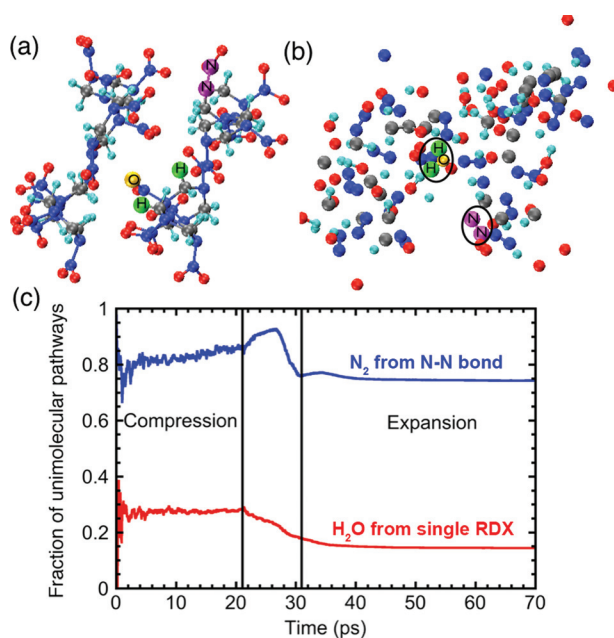


FIG. 3. (a) Initial configuration of RDX molecules in a unit cell, where gray, cyan, blue, and red spheres represent C, H, N, and O atoms, respectively. Atoms that later will be bonded to form N_2 and H_2O molecules are highlighted with different colors, i.e., H, O, and N are in green, yellow and magenta, respectively. (b) Molecular fragments formed behind the reversed shock front traveling rightward, where N_2 and H_2O molecules formed by the highlighted atoms in (a) are enclosed in circles. (c) Fraction of N_2 and H_2O molecules formed by atoms from single RDX molecules as a function of time.

RDX molecule in the initial configuration in Fig. 3(a), i.e., a unimolecular pathway. We have examined the origin of the other N_2 molecules as well, as shown in Fig. S3.⁴⁰ Interestingly, most of them are from N-N bonds within single RDX molecules, even though $-NO_2$ functional groups cleave first when the shock front passes RDX, as was seen in a previous simulation.¹⁵ Experimental results also indicate that NO_2 is a direct product of N-N hemolysis in the initial reaction stage under shock.⁴⁴

To better identify the source of the most abundant fragments (N_2 and H_2O), Fig. 3(c) plots the fraction of N_2 and H_2O molecules that are produced by unimolecular pathways, i.e., all constituent atoms of each molecule originate from a single RDX molecule in the initial configuration: $f_{\alpha}^{\text{intra}}$ ($\alpha = N_2, H_2O$). We see that N_2 production mechanism is predominantly unimolecular. Namely, 75% of the N_2 products are from N-N bonds within single RDXs. In contrast, only 15% of H_2O products are formed by H and O atoms from single RDXs, i.e., H_2O production mechanism is intermolecular. Figure S4 provides detailed analysis of the origin of the H and O atom of H_2O .⁴⁰ This implies that N atoms react locally, while H and O atoms move more actively to react with those from further non-adjacent RDX molecules. This is consistent with simulation results by Wu *et al.*,² who found a catalytic behavior of water in the detonation of HE. They found that H_2O actively participates in reactions by transporting oxygen between different fragments, instead of being a mere stable final product. The role of hydrogen as long-ranged reaction participants is understandable because of their lightest mass. Accordingly, H atoms can travel farther to bond with O atoms from other reactant molecules to form H_2O .

To understand the reaction pathways involving the rest of the elements (particularly carbon) and the reason behind the slow production of CO molecules, we study the time evolution of the population of large clusters remained in the system. Here, we define a large cluster as that containing more number of atoms than the 21-atom RDX molecule. Figure 4(a) shows the fraction N_C/N_T of the number of atoms in larger clusters, $N_C = \sum_{i>21} C(i)i$, vs. the total number of atoms in the system, $N_T = \sum_{i=1}^{\infty} C(i)i$, as a function of time. Here, $C(i)$ is the number of molecular fragments each consisting of i atoms. In the compression phase, the number of coagulated atoms, which are from the compressed part of RDX, increases linearly with time. Once no further shock loading is applied on the system, the large clusters start to decompose. Especially in the initial expansion phase, the sudden release from the right opening side leads to massive decomposition of the large clusters, which produce vast amount of small fragments such as N_2 and H_2O . However, in the later stage, lower temperature and density cannot sustain further chemical decomposition reactions. As a result, more than 10% of the atoms remain in large clusters even at the end of the total simulated time of 70 ps. The characteristic decay time of the large clusters is estimated by the exponential fitting as $\tau_{\text{decay}} = 800 \pm 500$ ps, which is close to the reaction time of CO: $\tau_{\text{CO}} = 900 \pm 400$ ps. Therefore, we can identify the large metastable clusters to be the major retardant of the CO-production reaction. Figure S5 provides more detailed analysis of the large clusters.⁴⁰

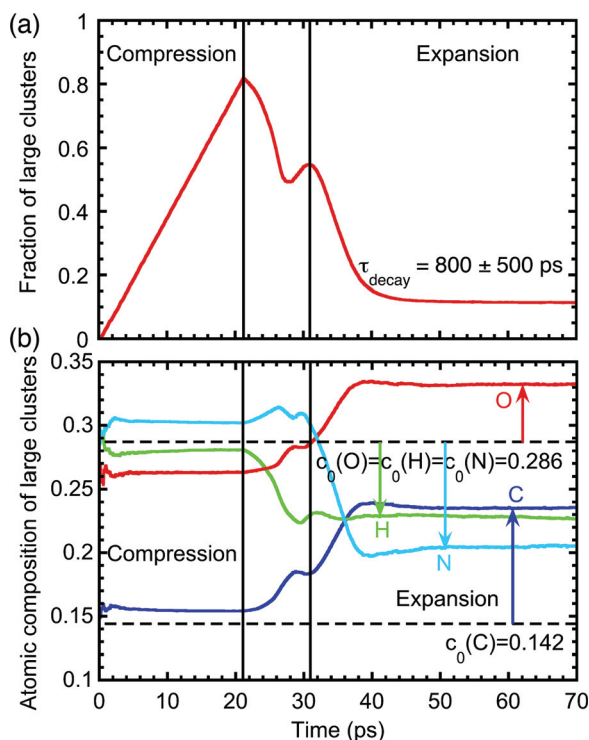


FIG. 4. Time evolution of large clusters. (a) Fraction of the number of atoms in larger cluster N_C vs. the total number of atoms in the system N_T . (b) Stoichiometric composition of the large clusters as a function of time. The dashed lines show the normalized stoichiometric number for different elements in the RDX molecule, $C_3H_6N_6O_6$. The arrows indicate how the stoichiometric value changed at the final state.

We next perform stoichiometric analysis of the large clusters. Figure 4(b) shows the averaged atomic compositions, $c(\alpha)$ ($\alpha = C, H, O, N$), of the large clusters as a function of time, which is normalized as $\sum_{\alpha} c(\alpha) = 1$. In the figure, the dashed lines show the composition for different elements in the RDX molecule: $c_0(C) = 3/21$ while $c_0(H) = c_0(O) = c_0(N) = 6/21$. Comparison of the compositions $c(\alpha)$ of the large clusters with those of the RDX reactant $c_0(\alpha)$ shows that the large clusters at the end of the simulation are not only carbon-rich but also oxygen-rich. Namely, the average stoichiometry of the large clusters at 70 ps is summarized as $C_{4.94}H_{4.76}O_{6.99}N_{4.31}$ (where the numbers are normalized to add up to 21—the number of atoms in an RDX molecule), which contains more C and O atoms than the RDX reactant, $C_3H_6O_6N_6$. Since these large C- and O-rich clusters remain metastable, it inhibits the formation of final CO products.

This mechanism of large C- and O-rich clusters as reaction retardants is akin to a recently proposed mechanism in another HE crystal, TATB. Manaa *et al.*⁶ found that N-rich clusters impede the formation of the final product of N_2 and solid carbon. Similarly, in our simulation of RDX, the persistent formation of large C- and O-rich clusters prohibit the formation of CO, which occur at different stages during the simulation. Carbon-rich clusters form immediately once the simulation starts. On the other hand, oxygen-rich clusters only form after the expansion phase; see Fig. 4(b). It can be seen in Fig. 4(b) that originally N-rich clusters also become N-poor during the expansion of the system. The change in composition slows down after 40 ps, consistent with the slow decay time (~ 1 ns) of the large clusters in Fig. 4(a). We

should note that similar C clusters were invoked to explain relative abundance of CO_2 products compared to CO at high densities in Ref. 42. However, our analysis shows a power-law decay of the cluster-size distribution and associated fractal nature of the clusters, indicating the necessity of large simulations to capture the essence of large clusters as was done in this paper (see Fig. S6).⁴⁰

In order to validate the metastability of the large C- and O-rich clusters in the high-temperature detonation condition, we perform QMD simulations, in which interatomic forces are computed quantum mechanically in the framework of density functional theory. We pick one of the carbon-rich clusters ($C_{12}H_{20}O_{13}N_{13}$) from the population of large clusters in the ReaxFF-MD simulation, and perform QMD simulations on them using the VASP software package⁴⁵ at a temperature of 1300 K in the canonical ensemble for 2 ps. In the simulations, electronic states are calculated using the projector-augmented-wave method.⁴⁶ The generalized gradient approximation⁴⁷ is used for the exchange-correlation energy. The plane-wave cutoff energy is set as 400 eV. Within the time period of the QMD simulation, the selected fragment remains stable (see the movie S1 in supplementary material⁴⁰).

In summary, our ReaxFF-MD simulations clearly revealed two time scales for the formation of final products of RDX during detonation. First, N_2 and H_2O (and OH) are formed rapidly within ~ 10 ps, resulting from uni- and intermolecular reaction pathways, respectively. Subsequently, CO starts to form at a very low rate (i.e., the reaction time ~ 1 ns). We found that the CO production is retarded by the formation of large C-rich and O-rich clusters. Such atomistic understanding of the reaction time and intermediate products provides valuable insight into broad technologies involving HEs. An example is rational design of insensitive energetic materials and detonation synthesis of materials such as nanodiamond.³

This work was supported by the Office of Naval Research Grant No. N000014-12-1-0555.

- ¹E. J. Reed, M. R. Manaa, L. E. Fried, K. R. Glaesemann, and J. D. Joannopoulos, *Nat. Phys.* **4**(1), 72 (2008).
- ²C. J. Wu, L. E. Fried, L. H. Yang, N. Goldman, and S. Bastea, *Nat. Chem.* **1**(1), 57 (2009).
- ³V. Pichot, B. Risse, F. Schnell, J. Mory, and D. Spitzer, *Sci. Rep.* **3**, 2159 (2013).
- ⁴D. W. Brenner, D. H. Robertson, M. L. Elert, and C. T. White, *Phys. Rev. Lett.* **70**(14), 2174 (1993).
- ⁵B. M. Rice, W. Mattson, J. Grosh, and S. F. Trevino, *Phys. Rev. E* **53**(1), 611 (1996).
- ⁶M. R. Manaa, E. J. Reed, L. E. Fried, and N. Goldman, *J. Am. Chem. Soc.* **131**(15), 5483 (2009).
- ⁷M. Losada and S. Chaudhuri, *J. Phys. Chem. A* **113**(20), 5933 (2009).
- ⁸M. Losada and S. Chaudhuri, *J. Chem. Phys.* **133**(13), 134305 (2010).
- ⁹M. S. Shaw and J. D. Johnson, *J. Appl. Phys.* **62**(5), 2080 (1987).
- ¹⁰L. Z. Zhang, S. V. Zybin, A. C. T. van Duin, S. Dasgupta, W. A. Goddard, and E. M. Kober, *J. Phys. Chem. A* **113**(40), 10619 (2009).
- ¹¹R. A. Yetter, F. L. Dryer, M. T. Allen, and J. L. Gatto, *J. Propul. Power* **11**(4), 683 (1995).
- ¹²J. E. Patterson, Z. A. Dreger, and Y. M. Gupta, *J. Phys. Chem. B* **111**(37), 10897 (2007).
- ¹³R. J. Hudson, P. Zioupos, and P. P. Gill, *Propellants, Explos., Pyrotech.* **37**(2), 191 (2012).
- ¹⁴T. Li, C. Hua, and Q. Li, *Propellants, Explos., Pyrotech.* **38**(6), 770 (2013).
- ¹⁵A. Strachan, A. C. T. van Duin, D. Chakraborty, S. Dasgupta, and W. A. Goddard, *Phys. Rev. Lett.* **91**(9), 098301 (2003).

- ¹⁶K. Nomura, R. K. Kalia, A. Nakano, P. Vashishta, A. C. T. van Duin, and W. A. Goddard, *Phys. Rev. Lett.* **99**(14), 148303 (2007).
- ¹⁷Q. An, Y. Liu, S. V. Zybin, H. Kim, and W. A. Goddard, *J. Phys. Chem. C* **116**(18), 10198 (2012).
- ¹⁸J. K. Brennan, M. Lisal, J. D. Moore, S. Izvekov, I. V. Schweigert, and J. P. Larentzos, *J. Phys. Chem. Lett.* **5**(12), 2144 (2014).
- ¹⁹D. Chakraborty, R. P. Muller, S. Dasgupta, and W. A. Goddard, *J. Phys. Chem. A* **104**(11), 2261 (2000).
- ²⁰Y. Zel'dovich, *Theory of Detonation* (Academic Press, 1960).
- ²¹A. J. B. Robertson, *Trans. Faraday Soc.* **45**(1), 85 (1949).
- ²²R. E. Duff and E. Houston, *J. Chem. Phys.* **23**(7), 1268 (1955).
- ²³S. N. L. Lubyatinsky and B. G. Loboiko, *AIP Conf. Proc.* **370**, 779 (1996).
- ²⁴A. P. Ershov and N. Satonkina, *Combust. Flame* **157**(5), 1022 (2010).
- ²⁵N. E. Ermolin, O. P. Korobeinichev, L. V. Kuibida, and V. M. Fomin, *Combust. Explos. Shock Waves* **24**(4), 400 (1988).
- ²⁶J. E. Davidson and M. Beckstead, *J. Propul. Power* **13**(3), 375 (1997).
- ²⁷R. A. Graham, *Solids under High-pressure Shock Compression* (Springer, 1993).
- ²⁸D. E. Hare, J. Franken, and D. D. Dlott, *Chem. Phys. Lett.* **244**(3–4), 224 (1995).
- ²⁹N. C. Dang, C. A. Bolme, D. S. Moore, and S. D. McGrane, *Phys. Rev. Lett.* **107**(4), 043001 (2011).
- ³⁰J. C. Crowhurst, M. R. Armstrong, K. B. Knight, J. M. Zaug, and E. M. Behymer, *Phys. Rev. Lett.* **107**(14), 144302 (2011).
- ³¹A. Tokmakoff, M. D. Fayer, and D. D. Dlott, *J. Phys. Chem.* **97**(9), 1901 (1993).
- ³²D. D. Dlott, *J. Phys. IV* **5**(C4), 337 (1995).
- ³³T. Germann and K. Kadau, *Int. J. Mod. Phys. C* **19**(9), 1315 (2008).
- ³⁴K. Nomura, R. K. Kalia, A. Nakano, and P. Vashishta, *Comput. Phys. Commun.* **178**(2), 73 (2008).
- ³⁵A. C. T. van Duin, S. Dasgupta, F. Lorant, and W. A. Goddard, *J. Phys. Chem. A* **105**(41), 9396 (2001).
- ³⁶T. T. Zhou, S. V. Zybin, Y. Liu, F. L. Huang, and W. A. Goddard, *J. Appl. Phys.* **111**(12), 124904 (2012).
- ³⁷L. Borne, J. Mory, and F. Schlessler, *Propellant, Explos., Pyrotech.* **33**(1), 37 (2008).
- ³⁸N. K. Bourne, *Shock Waves* **11**(6), 447 (2002).
- ³⁹Z. Liu, S. Nagano, and S. Itoh, *AIP Conf. Proc.* **505**, 227 (2000).
- ⁴⁰See supplementary material at <http://dx.doi.org/10.1063/1.4902128> for simulation details.
- ⁴¹A. C. T. van Duin, Y. Zeiri, F. Dubnikova, R. Kosloff, and W. A. Goddard, *J. Am. Chem. Soc.* **127**(31), 11053 (2005).
- ⁴²A. Strachan, E. M. Kober, A. C. T. van Duin, J. Oxgaard, and W. A. Goddard, *J. Chem. Phys.* **122**(5), 054502 (2005).
- ⁴³V. F. Anisichkin, *Russ. J. Phys. Chem. B* **5**(2), 304 (2011).
- ⁴⁴J. E. Patterson, Z. A. Dreger, M. S. Miao, and Y. M. Gupta, *J. Phys. Chem. A* **112**(32), 7374 (2008).
- ⁴⁵G. Kresse and J. Furthmuller, *Phys Rev B* **54**(16), 11169 (1996).
- ⁴⁶P. E. Blochl, *Phys. Rev. B* **50**(24), 17953 (1994).
- ⁴⁷J. P. Perdew, K. Burke, and M. Ernzerhof, *Phys. Rev. Lett.* **77**(18), 3865 (1996).